

Simple model of capillary condensation in cylindrical pores

Leszek Szybisz^{1,2,*} and Ignacio Urrutia^{1,†}¹Laboratorio TANDAR, Departamento de Física, Comisión Nacional de Energía Atómica, Avenida del Libertador 8250, RA-1429 Buenos Aires, Argentina²Departamento de Física, Facultad de Ciencias Exactas y Naturales, Universidad de Buenos Aires, Ciudad Universitaria, RA-1428 Buenos Aires, Argentina

(Received 10 April 2002; revised manuscript received 25 June 2002; published 13 November 2002)

A simple model based on an approximation of the dropletlike model is formulated for studying adsorption of fluids into cylindrical pores. This model yields a *nearly universal* description of capillary condensation transitions for noble gases confined by alkali metals. The system's thermodynamical behavior is predicted from the values of two dimensionless parameters: D^* (the reduced asymptotic strength of the fluid-adsorber interaction, a function of temperature) and R^* (the reduced radius of the pore). The phenomenon of hysteresis inherently related to capillary condensation is discussed. The connection to a previously proposed universality for cylindrical pores is also established.

DOI: 10.1103/PhysRevE.66.051201

PACS number(s): 61.20.-p, 68.03.Cd

I. INTRODUCTION

Capillary condensation (CC) consists of liquid condensation in porous media at pressures less than saturated vapor pressure (SVP). This phenomenon has been the subject of extensive experimental and theoretical investigations since many decades (see Refs. [1–11] and references cited therein). Figure 1 in Ref. [5] represents schematically the two most analyzed geometries, i.e., planar slits and cylindrical cavities. The slit pore consists of two flat parallel walls at a separation L_s , while cylindrical pores are characterized by its nominal radius R_p .

In some cases, the behavior of CC can be understood adequately in terms of the Kelvin equation (KE), which expresses the adsorption below SVP in terms of the liquid-vapor surface tension (σ_{lv}) and the size parameter of the confining walls (i.e., L_s or R_p). For large size parameters and strongly attracting walls, the error in using the KE is small [3,4]; then the KE can be corrected by taking into account that there is no fluid close to the walls due to the repulsive core of the adsorption potential. This approach does not suffice if the adsorption interaction is weak and/or the size parameter is small. In order to overcome this shortcoming, an alternative formulation has been proposed in Ref. [9]. In that paper, a simple model was devised and applied to planar slits predicting successfully the wide range of behavior that can occur.

As a natural extension of the simple model calculations of Ref. [9], its application to curved geometries where the surface energy plays an enhanced role became of interest. Such a description has been very recently utilized for studying the phase behavior of fluids in a regular array of infinitely long,

solid, parallel cylinders [12]. The authors of this work have found that for a rather compact distribution of cylinders, besides the well known film and capillary condensation phases, an additional necking configuration may appear. In the latter phase the fluid forms bridges or “necks” between neighboring cylinders. Along this line of investigations, in the present work we explore the possibility of applying a simple model for CC like that proposed in Ref. [9] to study cylindrical pores, completing in this way the regular geometries depicted in Ref. [5]. In doing so, cylindrical systems are treated on the basis of a schematic version of the dropletlike model reported in Refs. [13,14]. Like the KE, our model is derived from a simple set of assumptions and, therefore, sacrifices some degree of quantitative accuracy. However, the obtained results are very encouraging.

Besides the topics treated in Ref. [9], in this paper we shall also describe metastable phases and loops of hysteresis. As numerical applications we examined the adsorption of inert gases into pores of alkali metals. These systems are very interesting due to the fact that such substrates (Cs, Rb, K, Na, and Li) are much weaker attractors than surfaces of materials such as Al, Au, or graphite. Besides the very rich literature about the adsorption of quantum liquid ⁴He onto surfaces of alkali metals (see Refs. [15,16] and references quoted therein) one may currently observe an increasing effort for investigating the behavior of classical gases in presence of this kind of substrates [17]. The adsorption of Ne is the most studied one [18–22]. For instance, some evidence has been found for a drying behavior of Ne near a flat surface of Cs [18,22].

In the present work we seek for some universal properties of cylindrical pores made of different alkali metals filled with inert gases. Let us point out that the authors of Ref. [5] mainly compare the film thickness in the case of planar walls and cylinders for a given undersaturation. Universal features have been predicted in Refs. [3,4] on the basis of results obtained from calculations performed in a hydrodynamic model. Later in the text, we shall discuss the connection between our findings and predictions of Refs. [3,4].

The paper is organized in the following way. In Sec. II we

*Also at the Carrera del Investigador Científico of the Consejo Nacional de Investigaciones Científicas y Técnicas, Av. Rivadavia 1917, RA-1033 Buenos Aires, Argentina.

†Also at the Comisión de Investigaciones Científicas de la Prov. de Buenos Aires, Calle 526 entre 10 y 11, RA-1900 La Plata, Argentina.

outline the model. The numerical results are presented in Sec. III together with the discussion of the whole picture exhibited by the systems. Section IV is devoted to final remarks.

II. THE MODEL

The adsorption properties may be studied by analyzing the grand free energy,

$$\Omega[N] = F[N] - \mu N, \quad (2.1)$$

where F is the Helmholtz free energy, μ the chemical potential, and N the number of particles of the system. The value of temperature T is implicitly present in both Ω and F . For a cylindrical geometry, it is useful to describe the size of the system by the number of particles per unit length L , i.e., $n_\lambda = N/L$. For this symmetry the behavior is to be predicted by evaluating the equilibrium value of $n_\lambda^{\text{eq}} = N_{\text{eq}}/L$ as a function of μ . The value of n_λ^{eq} may be determined by minimizing Ω with respect to N . In terms of the parameters describing the system, there is a regime that exhibits no adsorption ($\Omega > 0$), a CC region, and a regime where a film is stable.

An expression for the Helmholtz free energy per particle for the CC phase, f_{CC} , may be obtained from the formalism developed in Refs. [13,14]. Assuming that the free energy of the fluid is given by the main contributions of the volume, surface, and substrate terms; then, if the fluid fills a pore forming a sharp cylinder of radius R_0 with density equal to the bulk equilibrium value ρ_0 , one gets

$$f_{\text{CC}} = \frac{F_{\text{CC}}}{N} = \frac{F_{\text{CC}}}{n_\lambda L} = f_\infty + 2 \sigma_{lv} \sqrt{\frac{\pi}{\rho_0}} n_\lambda^{-1/2} + 2 \pi \rho_0 \left\{ \int_0^{R_0} r dr U_{\text{sub}}(r) \right\} n_\lambda^{-1}, \quad (2.2)$$

with

$$N = \pi \rho_0 R_0^2 L. \quad (2.3)$$

Here f_∞ is the asymptotic value and it coincides with the chemical potential μ_0 at SVP. The relevant observables for bulk liquid ^4He at $T=0$ K and for the other noble gases Ne, Ar, Kr, and Xe at the corresponding triple points taken from Refs. [17,23–29] are collected in Table I.

The interaction between the filling atoms and the wall of a pore have been recently modeled [14]. In that work it is supposed that a pore gives rise to an $U_{\text{sub}}(r)$ equal to the sum of contributions yielded by successive concentric cylindrical shells, with radius R_{shell} , of atoms of the substrate,

$$U_{\text{sub}}(r) = \sum_s U_{\text{sub}}^{(s)}(r, R_{\text{shell}}), \quad (2.4)$$

where r is the distance from the axis of the pore. This procedure had been previously used by Stan and Cole [30] in accounting for the effect produced by multiwall carbon nanotubes. Moreover, this idea has been also adopted in Ref. [19] for constructing gas-solid potentials due to planar surfaces.

TABLE I. Experimental values of relevant observables for the inert gases in the liquid phase at the triple point and the lattice parameters of solid alkali metals.

System	T_t (K)	μ_0 (K)	ρ_0 (\AA^{-3})	σ_{lv} (K/ \AA^2)	Reference	
^4He	0 ^a	-7.15	0.02184		[23]	
					0.274 ± 0.003	[24,25]
					0.257 ± 0.001	[26]
					0.272 ± 0.002	[27]
Ne	24.55	-232	0.03694	3.98	[17,28,29]	
Ar	83.81	-930	0.02117	9.74	[17,28,29]	
Kr	115.76	-1342	0.01785	11.22	[17,28,29]	
Xe	161.39	-1907	0.01411	12.65	[17,28,29]	
			a (\AA)			
Cs			6.045		[33]	
Rb			5.585		[33]	
K			5.225		[33]	
Na			4.225		[33]	
Li			3.491		[33]	

^aThe data for ^4He correspond to $T=0$ K.

This assumption of additivity of the contributions omits many-body effects that would reduce the overall attraction [29]. Although alkali metals are delocalized and highly conducting systems, we expect that this simple and rather crude approximation be qualitatively adequate for the purpose of this paper. Furthermore, we assume that a filling atom interacts with a single substrate atom of a shell via an isotropic Lennard-Jones (LJ) pair potential with standard parameters ε_{LJ} and σ_{LJ} . The next assumption is the use of an azimuthally and longitudinally averaged potential. Under these conditions, it is possible to demonstrate that the total effect for a single shell is given by [see Eq. (2) in Ref. [30]]

$$U_{\text{sub}}^{(s)}(r, R_{\text{shell}}) = 3 \pi \Theta_s \varepsilon_{LJ} \sigma_{LJ}^2 \left[\frac{21}{32} \left(\frac{\sigma_{LJ}}{R_{\text{shell}}} \right)^{10} M_{11}(\nu) - \left(\frac{\sigma_{LJ}}{R_{\text{shell}}} \right)^4 M_5(\nu) \right], \quad (2.5)$$

where $\nu = r/R_{\text{shell}}$. In addition, Θ_s is the surface density of substrate atoms in a shell and it is determined by taking into account the crystallographic structure of the wall. Finally, $M_n(\nu)$ stands for the integral

$$M_n(\nu) = \int_0^\pi \frac{d\varphi}{(1 + \nu^2 - 2\nu \cos \varphi)^{n/2}}. \quad (2.6)$$

Of course, each approximation performed along this procedure introduces an error. However, we expect that the resulting potential would give a reliable description of the main features of the systems.

For all the inert gases, the substrate potentials produced by pores in different alkali metals were calculated using values of ε_{LJ} and σ_{LJ} determined by adjusting the pair potentials of Patil [31]. For this purpose, we followed the procedure utilized by Ancilotto *et al.* [32] for getting the He-alkali

TABLE II. Values of the LJ parameters for the interaction between noble gases and alkali metals, together with the asymptotic well depth and the location of the minimum corresponding to potentials given by Eqs. (2.4)–(2.6).

System	ε_{LJ} (K) ^a	σ_{LJ} (Å) ^a	r_m (Å)	D_∞ (K)	D^*
He-Cs	1.21	6.47	6.30	8.00	8.09
He-Na	1.73	5.40	5.22	17.97	15.07
He-Li	1.92	5.22	5.01	29.87	24.05
Ne-Cs	8.65	5.23	5.13	33.61	2.86
Ne-Na	11.94	4.37	4.26	72.38	5.11
Ne-Li	13.33	4.23	4.10	120.8	8.21
Ar-Cs	51.79	4.86	4.78	168.1	3.20
Ar-Na	60.32	4.20	4.10	330.9	5.41
Ar-Li	66.00	4.08	3.96	545.3	8.60
Kr-Cs	87.16	4.75	4.68	267.5	3.98
Kr-Na	94.10	4.16	4.06	504.1	6.20
Kr-Li	100.10	4.06	3.94	816.8	10.25
Xe-Cs	117.2	4.87	4.79	382.3	4.09
Xe-Na	126.0	4.27	4.10	720.6	6.60
Xe-Li	135.8	4.16	4.03	1179	10.61

^aParameters calculated with data taken from Ref. [31] by applying the procedure outlined in Ref. [32].

potentials from Patil's data. Quantity Θ_s was evaluated taking into account that solid alkali metals are bcc crystals with a lattice constants a listed in Table 3 of Ref. [33]. It was assumed that each shell coincides with a (100) plane of the crystalline structure, the first shell lies at the internal radius of the pore R_p , and the subsequent shells are located keeping an intershell distance equal to $a/2$. Following the assumption of Ref. [19] the sum is performed over four shells like in Eq. (3) therein. All the adopted parameters are quoted in Tables I and II.

In all the cases, for a pore with a certain radius R_p the potential $U_{\text{sub}}(r)$ exhibits a minimum with depth D_{R_p} at a distance r_m from the wall. It was found that for a given fluid-substrate combination, in the regime $R_p > \sigma_{LJ}$ the depth D_{R_p} decreases for increasing size of the pore (cf. Fig. 1 of Ref. [30]), while the location of r_m remains almost unchanged. Figures 1 and 2 show the typical behavior of D_{R_p} for several investigated systems as a function of the dimensionless inverse of the effective radius $R_0 = R_p - r_m$ defined as

$$1/(R_0/r_m) = 1/[(R_p - r_m)/r_m] = 1/(R^* - 1), \quad (2.7)$$

where

$$R^* = R_p/r_m. \quad (2.8)$$

In all these cases, D_{R_p} attains an asymptotic value D_∞ and the data are very well reproduced by the simple expression

$$D_{R_p} = D_{R^*} = D_\infty \left[1 + \frac{21}{32} \frac{1}{(R^* - 1)} - \frac{7}{128} \frac{1}{(R^* - 1)^2} \right]. \quad (2.9)$$

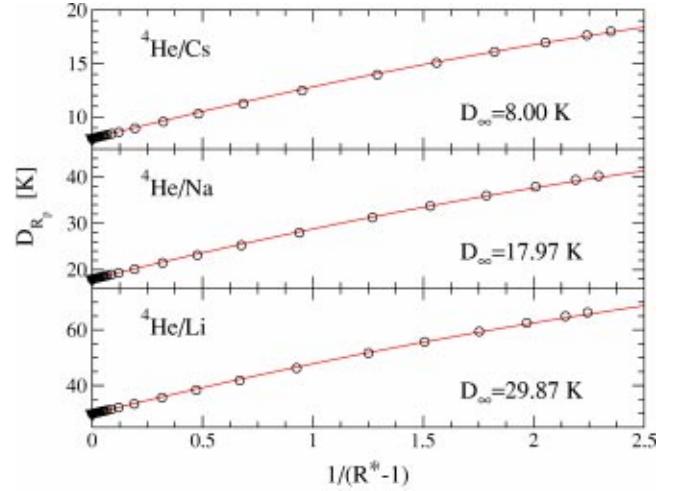


FIG. 1. Depth of the potential calculated with Eqs. (2.4)–(2.6) as a function of inverse of the reduced effective radius of the pores. Data for ^4He into cylindrical pores of Cs, Na, and Li are plotted. The corresponding asymptotic values D_∞ are given. Solid curves are the results provided by the simple expression (2.9).

The results for D_∞ and r_m are included in Table II. Since the results of calculations for adsorption into cavities in Rb and K do not differ qualitatively much from those for pores in Cs, the corresponding values are not included in this table. It is pertinent to mention that, for a given fluid-substrate system, r_m is larger than the corresponding parameter z_m for a slit geometry obtained from a 3–9 potential and listed in Table I of Ref. [9]. However, the values of r_m are close to z_m provided by a 4–10 potential utilized in Ref. [19] [e.g., for Ne/Cs one has $r_m = 5.13$, $z_m = 4.97$ (4–10 potential), and $z_m = 3.55$ Å (3–9 potential)].

A. Capillary condensed axial phase

Upon taking into account Eqs. (2.2) and (2.3), and the relation $R_0 = R_p - r_m$, the grand thermodynamic potential per unit length for the CC phase becomes

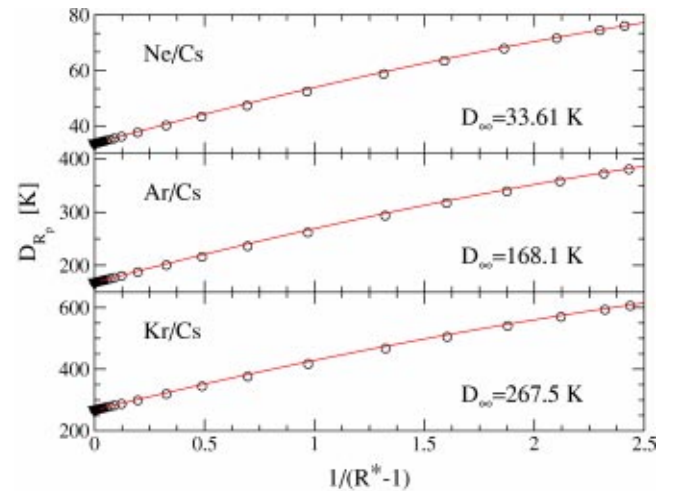


FIG. 2. Same as in Fig. 1, but for heavier noble gases into cylindrical pores of Cs.

$$\frac{\Omega_{CC}}{L} = \frac{F_{CC} - \mu N}{L} = 2 \pi \sigma_{lv} (R_p - r_m) + 2 \pi \rho_0 \int_0^{R_p - r_m} r dr \times U_{\text{sub}}(r) - \pi (\mu - \mu_0) \rho_0 (R_p - r_m)^2. \quad (2.10)$$

Furthermore, the grand thermodynamic potential per unit area of fluid's lateral surface for the CC phase may be written as

$$\frac{\Omega_{CC}}{A} = \frac{\Omega_{CC}}{2 \pi R_0 L} = \frac{F_{CC} - \mu N}{2 \pi (R_p - r_m) L} = \sigma_{lv} + \frac{\rho_0}{R_p - r_m} \times \int_0^{R_p - r_m} r dr U_{\text{sub}}(r) - \frac{1}{2} (\mu - \mu_0) \rho_0 (R_p - r_m). \quad (2.11)$$

Starting from this equation, it is possible to get the modified KE for CC. Upon defining the substrate-liquid interfacial tension σ_{sl} as the sum

$$\sigma_{sl} = \sigma_{lv} + \frac{\rho_0}{R_p - r_m} \int_0^{R_p - r_m} r dr U_{\text{sub}}(r) = \sigma_{lv} + I_U, \quad (2.12)$$

and setting $\Omega_{CC} = 0$, one arrives at

$$\sigma_{sl} - \frac{1}{2} (\mu - \mu_0) \rho_0 (R_p - r_m) = 0. \quad (2.13)$$

Next, by using the Gibbs-Duhem [34] relation for the fluid and neglecting any compression of the system, one gets

$$\rho_0 (\mu - \mu_0) = P - P_0, \quad (2.14)$$

which leads to the KE

$$2 \sigma_{sl} - (P - P_0) (R_p - r_m) = 0. \quad (2.15)$$

This equation expresses the pressure reduction for condensation in terms of the effective radius of the condensed fluid ($R_p - r_m$). The purpose of this work is to generalize the KE by taking into account both the explicit dependence on the substrate potential and the role of film formation on the adsorption behavior.

For the sake of generality, we shall follow the procedure of Ref. [9] discussing our predictions in terms of the dimensionless grand potential,

$$\Omega^* = \Omega / (A \sigma_{lv}). \quad (2.16)$$

When applying this normalization to Eq. (2.10), one must write the reduced version of the integrated adsorption potential per unit area, I_U . It is convenient to cast this contribution in the following form:

$$I_U^* = \frac{I_U}{\sigma_{lv}} = - \frac{D_\infty \rho_0}{\sigma_{lv} (R_p - r_m)} \int_0^{R_p - r_m} r dr [-U_{\text{sub}}(r) / D_\infty] = - \frac{1}{2} D^* g\{R^* - 1\}. \quad (2.17)$$

Here, we introduced the dimensionless integral

$$g\{y\} = \frac{1}{y} \int_0^y y' dy' [-U_{\text{sub}}(r_m y') / D_\infty], \quad (2.18)$$

with

$$y = r / r_m, \quad (2.19)$$

and the strength parameter is the reduced asymptotic well depth

$$D^* = 2 D_\infty r_m \rho_0 / \sigma_{lv}. \quad (2.20)$$

One immediately gets the reduced difference of chemical potentials,

$$\Delta = (\mu_0 - \mu) r_m \rho_0 / \sigma_{lv}. \quad (2.21)$$

The definitions of D^* and Δ are formally equal to that adopted in Ref. [9], where the authors use z_m instead of r_m .

Finally, one may write the reduced version of the grand potential given by Eq. (2.10) in the following way

$$\Omega_{CC}^* = 1 - \frac{1}{2} D^* g\{R^* - 1\} + \frac{1}{2} \Delta (R^* - 1). \quad (2.22)$$

This expression allows a study of adsorption in terms of D^* . The main difference between this result and that of Ref. [9] is a general factor 2 due to the fact that here Ω_{CC}/A is calculated by taking into account the whole lateral surface of the condensed liquid, while in the case of planar systems the area A corresponds to only one wall of the slit geometry. Before going ahead, let us remind that a fundamental property of the integral $g\{y\}$ introduced by Eq. (4) in Ref. [9] is its independence of the fluid-substrate combination. As we shall see below, this feature is also exhibited, to a very good approximation, by the integral $g\{y\}$ calculated according to Eq. (2.18).

B. Shell-film phase

Under the same assumptions adopted for writing Eqs. (2.2) and (2.10), the grand thermodynamic potential per unit length for a cylindrical film of thickness ℓ , i.e., for the shell-film (SF) phase, may be expressed as

$$\frac{\Omega_{SF}}{L} = \frac{F_{SF} - \mu N}{L} = 2 \pi \sigma_{lv} [(R_p - r_m - \ell) + (R_p - r_m)] + 2 \pi \rho_0 \int_{R_p - r_m - \ell}^{R_p - r_m} r dr U_{\text{sub}}(r) - \pi (\mu - \mu_0) \times \rho_0 [(R_p - r_m)^2 - (R_p - r_m - \ell)^2]. \quad (2.23)$$

Note that the film grows from $r = r_m$ towards the center. The reduced version of this grand free energy reads

$$\Omega_{\text{SF}}^* = \frac{\Omega_{\text{SF}}}{2\pi R_0 L \sigma_{lv}} = 2 - \frac{x}{R^* - 1} - \frac{1}{2} D^* \left[g\{R^* - 1\} - \left(1 - \frac{x}{R^* - 1}\right) g\{R^* - 1 - x\} \right] + \frac{1}{2} \Delta \left(2 - \frac{x}{R^* - 1}\right) x, \quad (2.24)$$

where x is the dimensionless thickness,

$$x = \ell / r_m, \quad (2.25)$$

which is related with the dimensionless inner radius y measured from the center of the cylinder,

$$y = (R_p - r_m - \ell) / r_m = R^* - 1 - x. \quad (2.26)$$

In this case, in order to find the stable configuration at fixed R^* (i.e., $R_p = \text{const}$), one must determine the value of x which provides the minimum Ω_{SF}^* .

III. GENERAL RESULTS—PHASE DIAGRAMS

A. Thresholds for CC and SF phases at SVP

The case of SVP ($\Delta = 0$) leads to a very simple criterion for the occurrence of CC. The expression for the transition line ($\Omega_{\text{CC}}^* = 0$) that separates the behavior into two regimes, capillary condensation ($\Omega_{\text{CC}}^* < 0$) or empty ($\Omega_{\text{CC}}^* > 0$), is

$$D_{\Delta=0}^*(\text{CC}) = \frac{2}{g\{R^* - 1\}}. \quad (3.1)$$

It coincides with Eq. (7) of Ref. [9] and its dependence on R^* is displayed in Fig. 3. In fact, the results obtained from calculations with potentials of the form of Eqs. (2.4)–(2.6) corresponding to different combinations of inert gases and substrates cannot be distinguished on the scale of the figure. Therefore, one can state that the curve given by Eq. (3.1) provides a *nearly universal* relation for the critical values of the parameters R^* and $D_{\Delta=0}^*$. However, it should be noticed that at SVP the transition from empty (E) to SF would occur for

$$D_{\Delta=0}^*(\text{SF}) = \frac{2(R^* - 1) + 2(R^* - 1 - x)}{(R^* - 1)g\{R^* - 1\} - (R^* - 1 - x)g\{R^* - 1 - x\}}. \quad (3.2)$$

It is clear that, for $0 < x < R^* - 1$, $D_{\Delta=0}^*(\text{SF})$ is always larger than $D_{\Delta=0}^*(\text{CC})$. So, for increasing D^* at SVP, when Ω_{SF}^* becomes zero then Ω_{CC}^* is already negative favoring the CC phase against the SF one.

Furthermore, the threshold condition for CC to occur at SVP for large R^* changes very little for increasing R^* , and for very broad pores attains the asymptotic value

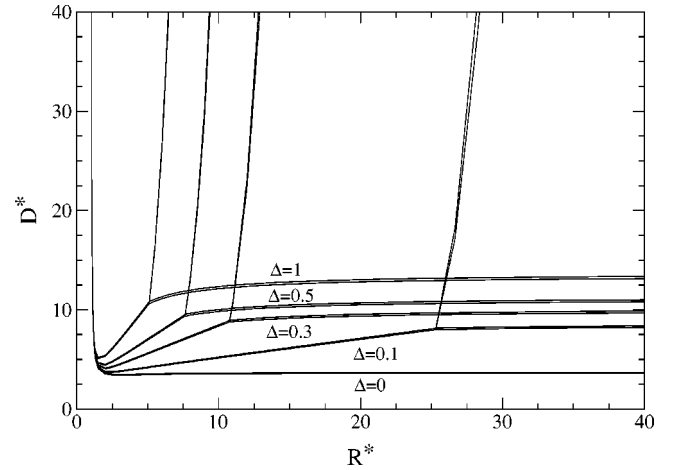


FIG. 3. Phase diagram present at varying degrees of undersaturation, expressed in terms of the reduced chemical potential difference Δ given by Eq. (2.21). For the case $\Delta = 0$, the line satisfies Eq. (3.1); all values above the curve correspond to capillary condensation, while those below are “empty.” For the other cases, $\Delta \neq 0$, there is a “triple point” below which the space is empty, to the upper right of which there is a shell film, and to the upper left there is capillary condensation (for more details see Fig. 5).

$$D_{\Delta=0}^*(\text{CC}; R^* \rightarrow \infty) = \lim_{R^* \rightarrow \infty} \left[\frac{2}{g\{R^* - 1\}} \right] \approx 3.7. \quad (3.3)$$

Perhaps this may be a surprising behavior because CC is typically found in small pores, while here it also occurs for broad cavities at $\Delta = 0$. Indeed, as we shall see later, *away from* SVP the domain of CC is restricted to narrow pores. At SVP, however, the energy balance in favor of CC is essentially maintained for increasing R^* because the magnitude of the integrated potential energy term also increases with R^* .

It is interesting to compare the asymptotic value of Eq. (3.3) with results provided by this simple model for planar substrates. The present value is slightly larger than that corresponding to the CC formation into the slit between two semi-infinite parallel solids separated by a reduced distance $L_s^* = L_s / z_m$ [see Eq. (10) in Ref. [9]]

$$D_{\Delta=0}^*(\text{CC}; L_s^* \rightarrow \infty) = \frac{32}{11} \approx 2.9. \quad (3.4)$$

The difference between the results for $D_{\Delta=0}^*(\text{CC}; R^* \rightarrow \infty)$ and $D_{\Delta=0}^*(\text{CC}; L_s^* \rightarrow \infty)$ is due to geometric effects, but also to the fact that the values of r_m and z_m are different as mentioned above. However, $D_{\Delta=0}^*(\text{CC}; R^* \rightarrow \infty)$ is considerably smaller than the wetting (W) transition condition for planar substrates

$$D_{\Delta=0}^*(W) = \frac{64}{11} \approx 5.8. \quad (3.5)$$

A glance at Table II indicates that for Ne and Ar adsorbed into pores of Cs it would not be possible to get the CC phase at $T = T_t$ because, in the present approach, the values $D^*[\text{Ne}/\text{Cs}] = 2.9$ and $D^*[\text{Ar}/\text{Cs}] = 3.2$ are smaller than 3.7.

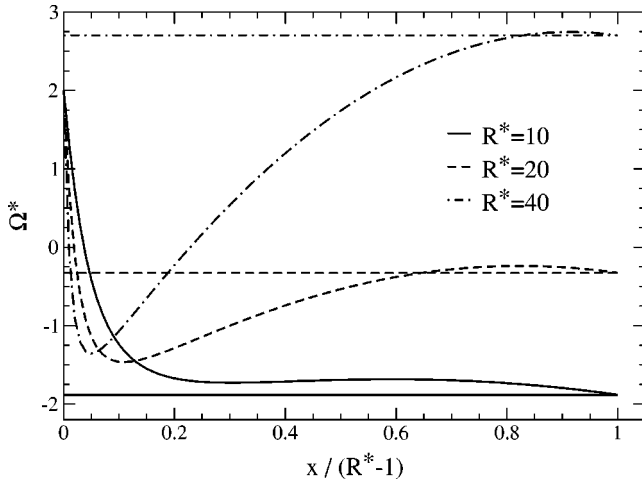


FIG. 4. Dimensionless grand potential Ω_{SF}^* (curved lines) as a function of normalized reduced thickness, $x/(R^*-1)$, compared with the values of Ω_{CC}^* (horizontal lines). The evaluations were done for $D^*=15.1$ (i.e., ${}^4\text{He}/\text{Na}$ in our approach) at $\Delta=0.3$ for a few values of R^* as indicated in the figure.

B. Thresholds for CC and SF phases below SVP

The general problem of behavior below SVP is more complicated. The presence of the Δ term in Eq. (2.22) leads to the following threshold value for CC:

$$D^*(\text{CC}) = D_{\Delta=0}^*(\text{CC}) \left[1 + \frac{1}{2} \Delta (R^* - 1) \right]. \quad (3.6)$$

However, one must now examine the possibility that a film configuration has a lower free energy than that of the CC phase. So, in the case $\Delta \neq 0$, it is necessary to evaluate the minimum of Ω_{SF}^* as a function of the variable x and to compare the result with Ω_{CC}^* . An example of this problem is displayed in Fig. 4. The difference between the grand free energy of the SF phase and that of the CC case written in terms of the dimensionless inner radius y is

$$\Omega_{SF}^* - \Omega_{CC}^* = \frac{y}{R^* - 1} \left(1 + \frac{1}{2} D^* g\{y\} - \frac{1}{2} \Delta y \right). \quad (3.7)$$

Here, the first term represents the extra surface energy of the film and the second represents the interaction between the solid surfaces and the atoms, which fill the gap when the SF to CC transition occurs; the third represents the free energy cost because the system is (in general) below SVP. When the internal radius of the shell film goes to zero, i.e., $y \rightarrow 0$, the difference of grand potentials given by Eq. (3.7) vanishes. This feature is clearly satisfied by results displayed in Fig. 4. This figure shows the behavior of Ω_{CC}^* and Ω_{SF}^* at $\Delta=0.3$ for three different pore sizes in the case $D^*=15.1$ (attributed to ${}^4\text{He}/\text{Na}$ in our approach). For all the considered cavities Ω_{SF}^* exhibits a minimum with a negative value. The situation is determined by the result for Ω_{CC}^* represented by horizontal lines. For the smallest radius, $R^*=10$, the CC is the stable phase because $\Omega_{CC}^* < \Omega_{SF}^*$, while the SF phase is metastable. For both larger radii, $R^*=20$ and 40 , the stable phase is a

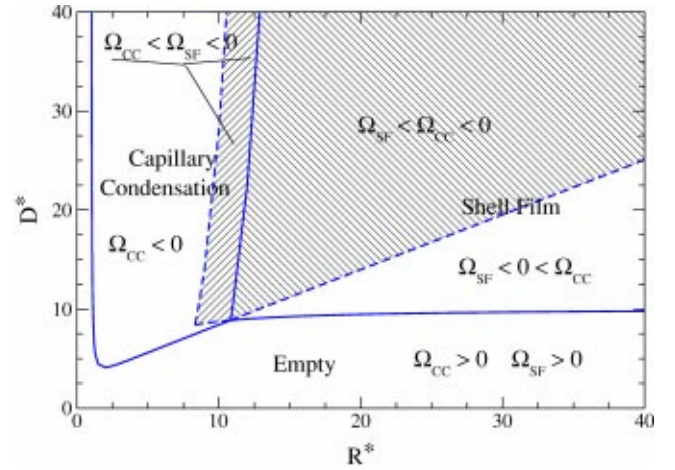


FIG. 5. Universal “phase diagram” showing regimes of empty, capillary condensed, and adsorbed shell film as a function of reduced pore radius and well depth defined in the text [see Eqs. (2.8) and (2.20)]. The displayed curves correspond to $\Delta=0.3$. The hatched zones are regions where both Ω_{SF}^* and Ω_{CC}^* are negative.

shell film at small $x/(R^*-1)$, while the CC phase presents different behaviors. For $R^*=20$ the CC phase is metastable and for $R^*=40$ it is unstable.

Before describing the phase diagram of the systems for any $\Delta \neq 0$, it is useful to look at further calculations for the case $\Delta=0.3$ treated above. Results obtained by varying D^* and R^* are plotted in Fig. 5, where some features of Ω_{CC}^* and Ω_{SF}^* are explicitly given. Solid lines separate domains of stable phases determined by following the procedure outlined when analyzing Fig. 4. The dashed straight line in the SF region is the threshold given by Eq. (3.6), while dashed curves in the CC regime denote the limit for SF solutions. So, the hatched zones indicate parameter regions where both CC and SF are negative. However, only that phase with lower Ω^* is stable, the other one is metastable and plays an important role in the cycle of hysteresis to be discussed later in the paper.

Let us now turn to the general phase diagram. The results for several values of Δ are displayed in Fig. 3, where only boundaries between stable phases are indicated. Indeed, the separations determined for different systems listed in Table II fall into very narrow bands confirming a *nearly universal* behavior. Increasing D^* favors SF or CC phases against the E phase. Which of the condensed phases is stable depends on R^* . For large R^* , SF is typically favored because of the cost of CC (the Δ term) becomes large relative to the benefits (from the potential and the decrease of surface tension). The SF to E transition curve is rather insensitive to R^* .

Figure 6 shows the reduced phase diagram projected onto the $R^*-\Delta$ plane for $D^*=15.1$ (i.e., corresponding to the case ${}^4\text{He}/\text{Na}$ already treated in other drawings). The curves indicate the transitions between stable phases. This plot also includes a few values obtained from Orsay-Paris nonlocal density-functional (OP-DF) calculations [14,35]. These results correspond to $R_p=13, 20, \text{ and } 30 \text{ \AA}$ and lie in the neighborhood of the “triple point” in this diagram, where the solutions are very sensitive to changes of Δ . Note that the

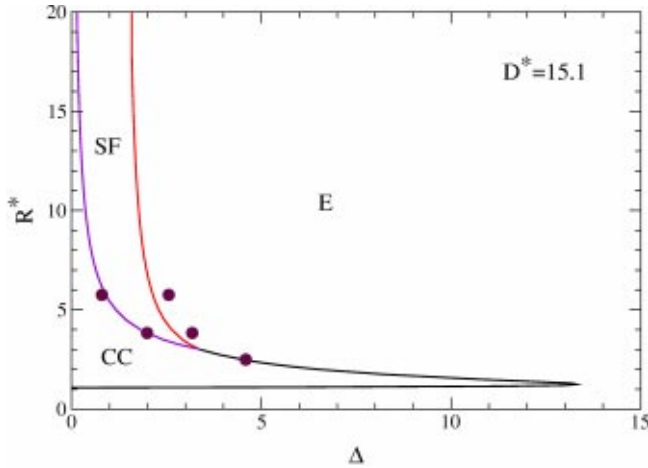


FIG. 6. Reduced phase diagram for $D^* = 15.1$ (i.e., ${}^4\text{He}/\text{Na}$ in our approach). The curves indicate the prediction for the boundaries among possible stable phases (empty, shell film, or capillary condensation). Note the existence of a “triple point.” The full circles stand for transitions determined from OP-DF calculations.

$E \rightarrow \text{SF}$, $\text{SF} \rightarrow \text{CC}$, and $E \rightarrow \text{CC}$ transitions occur in the OP-DF calculations at almost the same value of Δ as obtained in the simple model. Moreover, this agreement is similar to that found for planar systems (see Fig. 4 of Ref. [9]).

C. Temperature dependence

As mentioned above, for Ne/Cs and Ar/Cs the potential adopted in the present work leads to values of D^* at T_t markedly smaller than the asymptotic threshold $D_{\Delta=0}^*(\text{CC}; R^* \rightarrow \infty)$. This fact prevents the formation of the CC phase at T_t , but CC might be exhibited at higher temperatures. Therefore, it becomes important to examine the evolution of D^* for increasing temperatures. For this purpose one may follow the treatment of dimensionless quantities utilized for planar systems in Refs. [9,17]. Let us start by calculating the ratio of reduced depths given by Eq. (2.20) at two different temperatures,

$$\frac{D^*(T)}{D^*(T_t)} = \frac{2D_{\infty} r_m (\rho_{eq}/\sigma_{lv})_T}{2D_{\infty} r_m (\rho_0/\sigma_{lv})_{T_t}} = \frac{(\rho_{eq}/\sigma_{lv})_T}{(\rho_0/\sigma_{lv})_{T_t}}. \quad (3.8)$$

Here it is convenient to define

$$\mathcal{F}(T/T_t) = \frac{(\rho_{eq}/\sigma_{lv})_T}{(\rho_0/\sigma_{lv})_{T_t}} = \frac{(\sigma_{lv}/\rho_0)_{T_t}}{(\sigma_{lv}/\rho_{eq})_T}. \quad (3.9)$$

Selected values of the inverse of this ratio are displayed in Fig. 7. These data are located along a common line illustrating the fact that the right-hand side of Eq. (3.8) is a *universal* function of T/T_t . This means that the law of corresponding states [36,37] is obeyed. The whole domain of this law is restricted to the temperature range between the triple point and the critical point. The value $T_c/T_t = 1.85$ is provided by the Lennard-Jonesium model [29] and it agrees very well with experimental results for classical inert gases quoted in Table A.3 of that reference. However, due to the fact that in

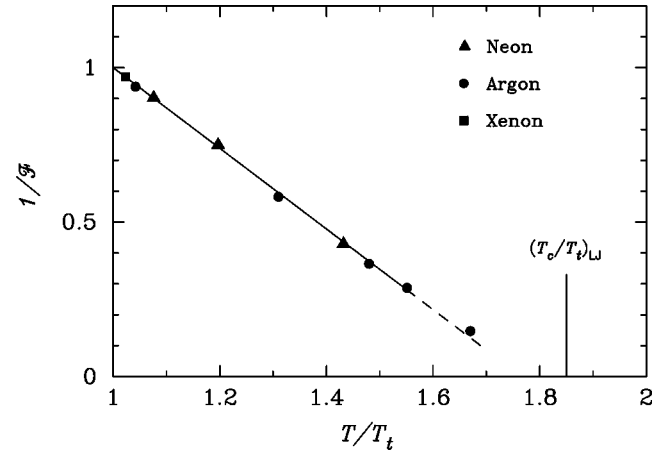


FIG. 7. Inverse of the ratio defined by Eq. (3.9) as a function of temperature ratio T/T_t . Selected data of inert gases Ne, Ar, and Xe illustrate the law of corresponding states.

our approach [see Eq. (2.2)] the influence of vapor is neglected, an important deviation could be present when the vapor density becomes bigger than 10% of the liquid density. This ratio of vapor/liquid densities is reached at about $T/T_t = 1.55$ for bulk Ne and Ar [20], therefore, for larger temperatures the line in Fig. 7 is dashed.

On the basis of results derived above by using the known asymptotic threshold reduced depth at the triple point it is possible to determine the value of D^* at any other T . From Eqs. (3.3) and (3.8) one may derive an implicit relation for the CC threshold at SVP,

$$D^*(T) = D^*(T_t) \mathcal{F}(T/T_t) = 3.7, \quad (3.10)$$

note that $D^*(T_t)$ corresponds to D^* listed in Table II. In the case of Ne/Cs this equality is satisfied at $T/T_t \approx 1.2$. Since this value lies inside the regime of validity of our model, one would get CC for $T \gtrsim 30$ K. For Ar/Cs the CC would be reached at even lower T/T_t .

D. Hysteresis

The phenomenon of hysteresis is inherently related to capillary condensation. There are numerous experimental evidences indicating that porous materials fill and drain at different values of the chemical potential leading to cycles of hysteresis. For instance, the reader may look at the data in Refs. [2,6,7,11].

Let us now outline the description of this phenomenon reported in Refs. [4,11]. Such a theoretical approach follows the main ideas of Preisach [38] first applied to magnetic materials, where there are also two-state elements. The Preisach model has been also adapted to treat other hysteretic systems. For instance, it was recently used for studying stress-strain hysteresis in rocks [39]. According to this interpretation a global hysteresis loop is a superposition of many hysteretic elements corresponding to noninteracting pores. It is assumed that a material has pores of different radii and that the size of these radii obeys a given statistical distribution. Each one of these pores is characterized by a pair of

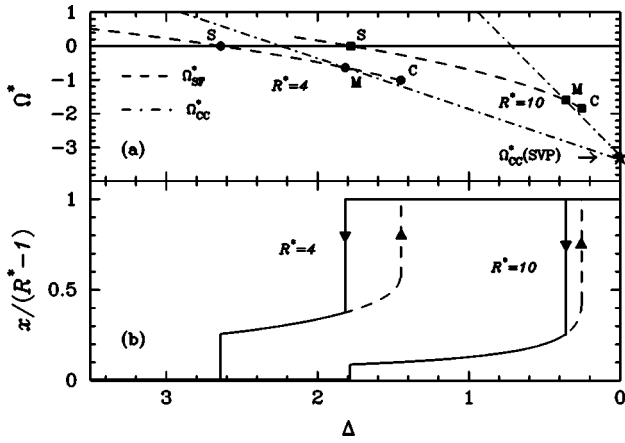


FIG. 8. (a) Reduced grand free energies for ${}^4\text{He}/\text{Na}$ ($D^* = 15.1$) for two different pore radii. Letter S indicates the beginning of the SF phase, while M and C are the critical points where the SF solutions become first metastable and next unstable. (b) Adsorption isotherms and loops of hysteresis. The solid curve corresponds to the adsorption along the configuration with minimum grand free energy. Probable filling and draining routes giving rise to elementary hysteretic cycles are shown with arrows.

chemical-potential values for filling (μ_α) and draining (μ_β), see Fig. 4 in Ref. [11]. A series of drawings reported in Fig. 5 of the latter reference illustrates how a cycle of hysteresis is traced out by averaging elementary contributions over the pore size distribution.

We shall now describe how the values of μ_α and μ_β corresponding to a single cylindrical pore can be determined from results provided by the examined simple model. In Fig. 8(a) we display the grand free energy of the phases SF and CC for ${}^4\text{He}/\text{Na}$ ($D^* = 15.1$) for two different pore radii, $R^* = 4$ and 10 . In both cases the results exhibit a similar pattern as a function of Δ . When μ approaches μ_0 from below, first of all, both Ω_{SF}^* and Ω_{CC}^* are positive, hence, the E phase is stable in this regime. Next, Ω_{SF}^* becomes negative at the critical point S giving rise to the transition $E \rightarrow \text{SF}$. For even smaller Δ , also Ω_{CC}^* becomes negative and eventually reaches lower values than Ω_{SF}^* , leading to the transition $\text{SF} \rightarrow \text{CC}$. This crossing occurs at Δ_M , which corresponds to a reduced film thickness x_M . Finally, at some critical values Δ_C and x_C the solution for SF becomes unstable. This sequence of facts can be also followed by exploring Figs. 3 and 5. Figure 8(b) shows the adsorption isotherms determined by successive stable phases, steps in the solid lines correspond to the above-mentioned transitions. It is worthy of notice that similar features have been found in the study of the adsorption in regular arrays of cylinders as shown in Fig. 4 of Ref. [12].

As mentioned before, in the literature it is assumed that the filling and draining of these single cylindrical cavities do not always follow the path guided by stable phases. In fact, the systems exhibit a sort of memory, trying to remain in the initial phase when Δ is changed giving rise to an elementary loop of hysteresis. The adsorption begins with the formation of a stable thin shell film that grows up to the crossing of Ω_{SF}^* with Ω_{CC}^* . The key assumption for building an elemen-

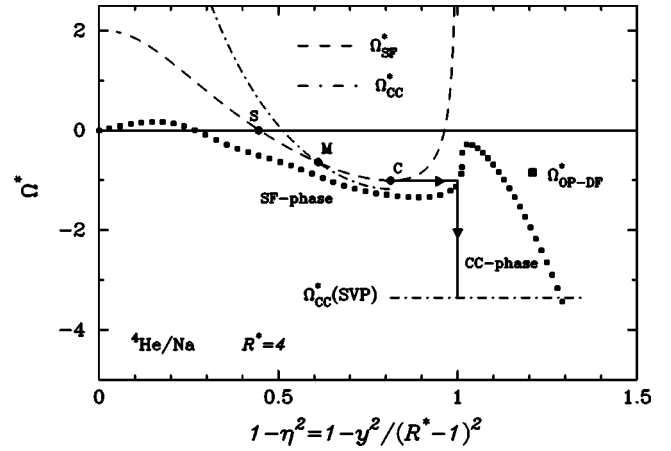


FIG. 9. Reduced grand free energy as a function of the filling factor $1 - \eta^2$ for the adsorption of ${}^4\text{He}/\text{Na}$ in case of $R^* = 4$. Results provided by the simple model and by OP-DF calculations are shown.

tary hysteretic loop [3,4,6,11] is that after this crossing the filling follows the metastable SF phase up to the critical point (Δ_C, x_C) where this sort of configuration becomes unstable. Then there is a vertical jump to the CC phase at $\Delta_C \equiv (\mu_0 - \mu_\alpha)r_m\rho_0/\sigma_{lv}$, as indicated by dashed lines in Fig. 8(b). It is clear that this choice is actually an upper limit in terms of x . Turning to the desorption, the authors of the above-mentioned references suggest that emptying occurs along the stability line. This means that there is a vertical jump from $x/(R^* - 1) = 1$ to x_M at $\Delta_M \equiv (\mu_0 - \mu_\beta)r_m\rho_0/\sigma_{lv}$.

The elementary cycles of hysteresis depicted in Fig. 8(b) for $R^* = 4$ and 10 indicate that for decreasing radius the cycle becomes broader. This is in agreement with the trend shown by results displayed in Fig. 6 of Ref. [4]. Experimental data on global hysteresis do not show the abrupt changes exhibited by the curves for elementary loops. The smearing is obtained when one averages over the pore size distribution as shown in Fig. 8 of Ref. [4].

The different physical situations that occur when one goes over the elementary hysteretic loop described above are depicted in Fig. 3 of Ref. [6] and comprehensively discussed in the corresponding text. In order to get more insight into the problem, we shall look at the evolution of the reduced grand free energy when a single perfect cylindrical pore is filled. This can be conveniently done by studying Ω^* yielded by the simple model as a function of the filling fraction evaluated at constant density,

$$\frac{(R_p - r_m)^2 - (R_p - r_m - \ell)^2}{(R_p - r_m)^2} = 1 - \frac{y^2}{(R^* - 1)^2} = 1 - \eta^2. \quad (3.11)$$

The results for the adsorption of ${}^4\text{He}$ into a $R^* = 4$ pore of Na are shown in Fig. 9, where S , M , and C are the critical points mentioned before. According to the description outlined above, the evolution of the SF phase up to the metastable point M runs over stable states. It should be stressed that to get the CC phase a rather macroscopic deformation of

the SF phase is required. Since between the points M and C the energy difference is small, it is plausible to assume that the system will undergo a macroscopic deformation just at C where Ω_{SF}^* exhibits the beginning of a very steep energy barrier and the SF becomes unstable. After reaching the critical point C the adsorption continues at constant Δ up to $\eta = 0$ as indicated by the horizontal solid line. This physical situation is shown in configuration II of Fig. 3 in [6], where one may observe the coexistence of SF and CC phases. Then, by decreasing Δ along the displayed vertical line the system will eventually reach $\Omega_{CC}^*(SVP)$.

For the sake of comparison we include in Fig. 9 the data obtained from OP-DF calculations [14]. In this case, like in planar geometry, the density profile of the fluid is not constant and presents a density peak close to the wall of the pore. This feature causes that more material, than according to the simple model, could be stored before the SVP conditions with $\mu = \mu_0$ are reached. Note that Ω^* yielded by OP-DF calculations for perfect cylindrical pores also exhibits an energy barrier between the SF and CC phases, which at adsorption would cause a domain of coexistence with a delay of the SF \rightarrow CC jump.

Looking at Fig. 9, one can state that the simple model provides a schematic approach to the OP-DF results.

E. Comparison with results of Cole and Saam

Let us now make a comparison between our results for x_M and x_C and the critical values obtained in Refs. [3,4]. In those papers it has been assumed that the adsorption potential $U_{sub}(r)$ is given by a sum of pair interactions containing only the attractive contribution $-C_6/|\vec{r}-\vec{R}_s|^6$ of a Lennard-Jones potential. This sum over the substrate atoms located at \vec{R}_s is, indeed, replaced by an integration over a continuum. The radial integral running over R_s is evaluated from $R_s = R_p - r_m$ to $R_s \rightarrow \infty$, yielding an expression in terms of a hypergeometric function. Under such conditions the authors of Refs. [3,4] determined the critical values of the inner radius at which the vertical isotherms should appear. We should recall that in the present work instead of integrating over R_s we sum over a few concentric shells.

Notice that, due to the assumptions made for evaluating the adsorption potentials, the pore radius of Refs. [3,4] is equivalent to the present effective pore radius $R_0 = R_p - r_m$. Then the relation between the inner radius a_{CS} defined in those references and the variables used in the present work is

$$\frac{a_{CS}}{R_p - r_m} = \frac{y}{R^* - 1} = 1 - \frac{x}{R^* - 1} = \eta. \quad (3.12)$$

Cole and Saam have shown that the critical values η_C and η_M lie on a universal curve as a function of a dimensionless variable defined as the ratio of the effective pore radius and a quantity related to the strength of the adsorption potential. Figure 2 in Ref. [3] shows the corresponding behavior. In order to facilitate a comparison we reproduce such curves in

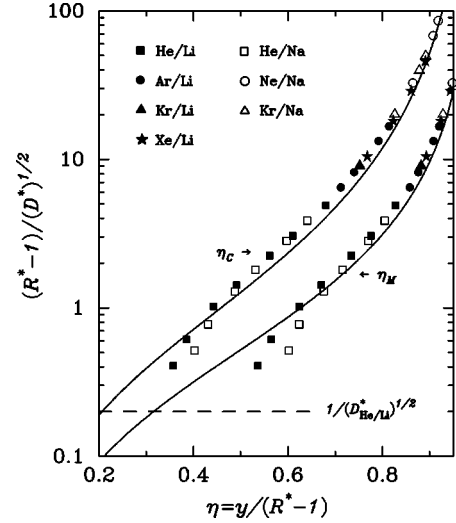


FIG. 10. Nearly universal correspondence of critical values of reduced inner radii η_M and η_C and the dimensionless ratio of effective radius and potential strength $(R^* - 1)/\sqrt{D^*}$. The solid curves are universal functions proposed in Ref. [3], which are discussed in the text.

the present Fig. 10. The evaluation has been done by using the explicit Eqs. (10) and (11) of Ref. [6].

Turning to the examined simple model, the appropriate equivalent dimensionless variable that carries information on the pore radius and the potential strength can be built in the following way:

$$\frac{R_p - r_m}{R_D} = \frac{R^* - 1}{\sqrt{D^*}}. \quad (3.13)$$

Figure 10 shows the correspondence between the critical values η_C and η_M and the dimensionless quantity $(R^* - 1)/\sqrt{D^*}$ obtained for several adsorbate-substrate combinations. One may realize that the data lie along *nearly* universal curves, which are close to that determined in Ref. [3]. The observed differences between both series of results can be mainly attributed to the above-mentioned different assumptions adopted for evaluating the adsorption potential. The marked falling down of the data for ${}^4\text{He}/\text{Na}$ and ${}^4\text{He}/\text{Li}$ calculated at $R^* = 3$ deserves a special consideration. Notice that in such cases R_p is not very much larger than σ_{LJ} . Curves plotted in Fig. 1 of Ref. [30] suggest that under such circumstances the shape of the adsorption potential given by Eq. (2.5) becomes different from that corresponding to wide pores. Therefore, on the basis of this feature one would expect a departure from the model of Ref. [3]. The dashed line in Fig. 10 corresponds to an estimation of the lowest limiting value of $(R^* - 1)/\sqrt{D^*}$ which could be achieved with systems composed of adsorbed inert gases into pores of alkali metals according to Fig. 3 and data of Table II.

IV. FINAL REMARKS

A simple model based on a proposal of Ref. [9] is applied for studying phase transitions in the case of adsorption into isolated cylindrical cavities. This model yields a *nearly uni-*

versal description of capillary condensation transitions for noble gases confined in pores of alkali metals providing an interpretation of the wide range of behavior that can occur.

This *quasiuniversality* is due to properties of the adsorption potential contributing to $g\{y\}$. Indeed, in the case of only one shell, the potential of Eq. (2.5) is a *universal* function of r/σ_{LJ} . This feature is very little perturbed when one defines reduced distances as r/r_{\min} because σ_{LJ}/r_{\min} is almost constant for all the examined liquid/substrate combinations. Furthermore, the inclusion of a few shells located at different distances $a/2$ leaves the position of r_{\min} almost unchanged.

The phase diagram for cylindrical pores displayed in Fig. 3 is qualitatively equivalent to that previously obtained in the literature for a slit geometry (see Fig. 2 in Ref. [9]). Furthermore, the reliability of the examined simple model is supported by results obtained from OP-DF calculations. Figure 6 shows that the transitions between stable phases occur in the OP-DF theory at virtually the same value of Δ as found in the simple model.

According to our calculation neither Ne nor Ar would form CC into pores of Cs at T_i , i.e., when the surface tension σ_{lv} is maximum. However, at $T/T_i \approx 1.2$ the CC may be formed in both cases because at that temperature the surface tension would have already decreased enough to favor CC against E . This feature resembles results obtained from calculations for these inert gases adsorbed onto planar Cs [19–22] and for Ne located between parallel walls of Cs [9]. So, we can state that in spite of the fact that the adsorption potentials proposed in the present work are, indeed, a first ap-

proximation to the problem, they are good enough to detect some features of Ne and Ar already observed at $T \approx T_i$ in the case of other geometries.

In examining the adsorption and desorption characteristics of cylindrical cavities on the basis of results obtained within the studied simple model, we also made a connection to the phenomenon of hysteresis. A global cycle of hysteresis can be interpreted by averaging contributions of single hysteretic elements [4,11]. It is shown how the critical variables of an elementary loop of hysteresis can be determined within the framework of the analyzed model. The results plotted in Fig. 10 indicate that the obtained critical radii for metastable phases and unstable films lie close to the previously proposed universal curves [3,4]. So, the adsorption potentials built up by adopting different assumptions, discussed in the text, lead to a qualitatively similar behavior. Finally, it should be noticed that experiments are not carried out with perfect cylindrical channels. In practice, there are irregularities such as those shown in Fig. 1 of Ref. [40]. If the deformations produce modulations of about 10% in the diameter of the cylinders, drops would nucleate and grow at each minimum in the diameter, and the nature of hysteresis would be changed significantly.

ACKNOWLEDGMENT

This work was supported in part by the Ministry of Culture and Education of Argentina through Grants PIP-CONICET No. 2000 and SIP No. EX-01/X103.

-
- [1] B.V. Derjaguin, Zh. Fiz. Khim. **14**, 137 (1940) [Acta Physicochim. URSS **12**, 181 (1940)].
- [2] D.F. Brewer and D.C. Champeney, Proc. Phys. Soc. London **79**, 855 (1962).
- [3] M.W. Cole and W.F. Saam, Phys. Rev. Lett. **32**, 985 (1974).
- [4] W.F. Saam and M.W. Cole, Phys. Rev. B **11**, 1086 (1975).
- [5] R. Evans and U.M.B. Marconi, Chem. Phys. Lett. **114**, 415 (1985).
- [6] D.T. Smith, K.M. Godshalk, and R.B. Hallock, Phys. Rev. B **36**, 202 (1987).
- [7] K.M. Godshalk and R.B. Hallock, Phys. Rev. B **36**, 8294 (1987).
- [8] E. Cheng, M.R. Swift, and M.W. Cole, J. Chem. Phys. **99**, 4064 (1993).
- [9] S.M. Gatica, M.M. Calbi, and M.W. Cole, Phys. Rev. E **59**, 4484 (1999).
- [10] M.M. Calbi, F. Toigo, S.M. Gatica, and M.W. Cole, Phys. Rev. B **60**, 14 935 (1999).
- [11] M.P. Lilly and R.B. Hallock, Phys. Rev. B **63**, 174503 (2001).
- [12] S. M. Gatica, M. M. Calbi, and M. W. Cole, Phys. Rev. E **65**, 061605 (2002).
- [13] L. Szybisz, Physica A **283**, 193 (2000).
- [14] L. Szybisz and S.M. Gatica, Phys. Rev. B **64**, 224523 (2001).
- [15] L. Szybisz, Phys. Rev. B **62**, 3986 (2000); **62**, 12 381 (2000).
- [16] F. Ancilotto, F. Faccin, and F. Toigo, Phys. Rev. B **62**, 17 035 (2000).
- [17] E. Cheng, M.W. Cole, W.F. Saam, and J. Treiner, Phys. Rev. B **48**, 18 214 (1993).
- [18] G.B. Hess, M.J. Sabatini, and M.H.W. Chan, Phys. Rev. Lett. **78**, 1739 (1997).
- [19] M.J. Bojan, G. Stan, S. Curtarolo, W.A. Steele, and M.W. Cole, Phys. Rev. E **59**, 864 (1999).
- [20] F. Ancilotto and F. Toigo, Phys. Rev. B **60**, 9019 (1999).
- [21] S. Curtarolo, G. Stan, M.J. Bojan, M.W. Cole, and W.A. Steele, Phys. Rev. E **61**, 1670 (2000).
- [22] F. Ancilotto, S. Curtarolo, F. Toigo, and M.W. Cole, Phys. Rev. Lett. **87**, 206103 (2001).
- [23] S. Stringari and J. Treiner, Phys. Rev. B **36**, 8369 (1987).
- [24] H.M. Guo, D.O. Edwards, R.E. Sarwinski, and J.T. Tough, Phys. Rev. Lett. **27**, 1259 (1971).
- [25] D.O. Edwards and W.F. Saam, in *Progress in Low Temperature Physics*, edited by D.F. Brewer (North-Holland, Amsterdam, 1978), Vol. 7A, Chap. 4.
- [26] M. Iino, M. Suzuki, and A.J. Ikushima, J. Low Temp. Phys. **61**, 155 (1985).
- [27] P. Roche, G. Deville, N.J. Appleyard, and F.I.B. Williams, J. Low Temp. Phys. **106**, 565 (1997).
- [28] S.-T. Wu and G.-S. Yan, J. Chem. Phys. **77**, 5799 (1982).
- [29] L.W. Bruch, M.W. Cole, and E. Zaremba, *Physical Adsorption* (Oxford Univ. Press, Oxford, 1997).
- [30] G. Stan and M.W. Cole, Surf. Sci. **395**, 280 (1998).

- [31] S.H. Patil, J. Chem. Phys. **94**, 8089 (1991).
- [32] F. Ancilotto, E. Cheng, M.W. Cole, and F. Toigo, Z. Phys. B: Condens. Matter **98**, 323 (1995).
- [33] C. Kittel, *Introduction to Solid State Physics* (Wiley, New York, 1986), Chap. 1.
- [34] J.S. Rowlinson and B. Widom, *Molecular Theory of Capillarity* (Clarendon Press, Oxford, 1982).
- [35] J. Dupont-Roc, M. Himbert, N. Pavloff, and J. Treiner, J. Low Temp. Phys. **81**, 31 (1990).
- [36] S.-K. Ma, *Statistical Mechanics* (World Scientific, Singapore, 1985).
- [37] R.K. Pathria, *Statistical Mechanics* (Butterworth-Heinemann, Oxford, 1996).
- [38] F. Preisach, Z. Phys. **94**, 277 (1935).
- [39] R.A. Guyer, K.R. McCall, and G.N. Boitnott, Phys. Rev. Lett. **74**, 3491 (1995).
- [40] J.M. Valles, Jr., D.T. Smith, and R.B. Hallock, Phys. Rev. Lett. **54**, 1528 (1985).